Topological Network Modes in a Twisted Moiré Phononic Crystal

Dan Yao,[1] Liping Ye,[1,*] Zhonghao Fu,[1] Qing Wang,[1] Hailong He,[1] Jiuyang Lu,[1,2] Weiyin Deng,[1,2] Xueqin Huang,[2] Manzhu Ke,[1] and Zhengyou Liu[1,3,†]

[1]*Key Laboratory of Artificial Micro- and Nanostructures of Ministry of Education and School of Physics and Technology, Wuhan University, Wuhan 430072, China*

[2]*School of Physics and Optoelectronics, South China University of Technology, Guangzhou, 510640, China*

[3]*Institute for Advanced Studies, Wuhan University, Wuhan 430072, China*

(Received 11 October 2023; revised 11 April 2024; accepted 21 May 2024; published 27 June 2024)

Twisted moiré materials, a new class of layered structures with different twist angles for neighboring layers, are attracting great attention because of the rich intriguing physical phenomena associated with them. Of particular interest are the topological network modes, first proposed in the small angle twisted bilayer graphene under interlayer bias. Here we report the observations of such topological network modes in twisted moiré phononic crystals without requiring the external bias fields. Acoustic topological network modes that can be constructed in a wide range of twist angles are both observed in the domain walls with and without reconstructions, which serve as the analogy of the lattice relaxations in electronic moiré materials. Topological robustness of the topological network modes is observed by introducing valley-preserved defects to the network channel. Furthermore, the network can be reconfigured into two-dimensional patterns with any desired connectivity, offering a unique prototype platform for acoustic applications.

DOI: 10.1103/PhysRevLett.132.266602

Twisted moiré materials, formed by two-dimensional (2D) material layers with twist angles between layers, exhibit moiré patterns varied with twist angle. Tuned by the moiré interlayer coupling and twist angle degrees of freedom, these moiré systems exhibit a plethora of interesting physics [1–15], such as van Hove singularities [1,3], moiré excitons [7,8], and topological phases [9–12]. Physics arising from twisted moiré electronic systems has opened a new field dubbed as twistronics. Of special interest is the twisted bilayer graphene formed by two graphene layers with a relative twist angle. Such systems typically exhibit triangular moiré patterns consisting of three regions of AA, AB, and BA stackings, where the AB and BA stacking regions are separated by domain wall (DW) forms. Their moiré patterns result in a strong modification of the electronic structure by the superlattice band folding, leading to emergent superconducting and correlated insulating states [5,6]. When a large interlayer bias is applied to a twisted bilayer graphene, the top and bottom graphene layers carry asymmetric potentials. The corresponding AB and BA regions open band gaps, characterized by opposite valley Chern numbers, supporting the presence of the valley topological modes in the DWs [11,15–27]. These topological modes form a connected network that provides a platform for performing complex valleytronic operations, such as Fabry-Pérot [19] and Aharanov-Bohm oscillations [23]. However, these topological network modes (TNMs) are only observed in the DWs of reconstructed structures of twisted bilayer graphene [19–26]. This happens only in small twist angles (e.g., less than 1°), due to the spontaneous lattice reconstruction, a necessary condition for realizing the TNMs in twisted bilayer graphene.

Inspired by the moiré electronic systems, some artificial moiré lattices of classical waves have been realized recently [28–45], in which some salient phenomena have been demonstrated, such as moiré flat bands [28,29,33–36,38], moiré fringe induced gauge field [30,40], moiré quasi-bound states [41,42], and localization and delocalization of light [43]. Although progress has been made in classical wave moiré systems, the studies on inherent topology and associated topological modes (e.g., TNMs) in classical wave moiré systems are rare and highly desirable. Classical wave moiré systems remain in a large unexplored realm.

Here we construct TNMs in twisted moiré phononic crystals (TMPCs). Because of their macroscopic scale, the DW structures and interlayer couplings of TMPCs can be flexibly designed and accurately fabricated with both large and small twist angles. Acoustic TNMs are observed by directly measuring the pressure field distribution in TMPCs. The topological robustness of TNMs is identified by introducing a weak defect, referred to as valley-preserved (VP) defect, which does not introduce valley mixing into the channel of the network. Significantly, the connectivity of the channels of the network can be blocked by a strong defect, referred to as valley-mixed (VM) defect, which introduces valley mixing. As such, we can design network waveguides of arbitrary shapes and guide the TNMs along any prescribed routes, which are conclusively identified by our acoustic experiments. Our results provide insight into the study of topological domain physics in

twisted systems as well as an effective macroscopic platform for exploring the highly intricate moiré physics.

Approach toward acoustic TNMs.—Before delving into the details of our TMPCs, we first briefly describe the design principle of our TNMs. Following the results demonstrated in the electronic systems [16–27], the key to obtaining TNMs is to let the top and bottom layers of the twisted system carry asymmetric potentials, which leads to the AB and BA regions of the system opening band gaps and exhibiting opposite valley Chern numbers. In this context, we start with 2D acoustic analog of graphene monolayer systems with potentials $\mathrm{V} \pm \Delta\mathrm{V}$, referred to as acoustic graphene layers. As illustrated in Fig. 1(a), two acoustic graphene layers are constructed following the Hamiltonians $H_{\pm} = (\mathrm{V} \pm \Delta\mathrm{V})\sigma_0 + d_1\sigma_x + d_2\sigma_y$ of the usual ones of the graphene, where $d_1 = t[1 + 2\cos(k_x/2)\cos(\sqrt{3}/2)k_y]$, $d_2 = 2t\cos(k_x/2)\sin(\sqrt{3}/2)k_y$, and the Hamiltonian H_- (H_+) correspond to the top (bottom) layer. These two acoustic graphene layers support Dirac points of frequencies f_1 (top layer) and f_2 (bottom layer) at the inequivalent hexagonal Brillouin zone corners K_0 and K_0', see Supplemental Material [46]. We then stack these two acoustic graphene layers in the vertical direction and create a TMPC by a twisting procedure sketched in Fig. 1(a). As shown in Fig. 1(b), the TMPC exhibits a triangular moiré pattern in the local stacking that smoothly alternates between three basic stacking types AA, AB, and BA. Hybridized with the interlayer coupling, the AB and BA regions of our TMPC develop spectral gaps and possess opposite valley Chern numbers [46], similar to the twisted bilayer graphene with a large interlayer bias applied [16–27]. Naturally, topologically protected modes appear at the DWs between the AB and BA regions, giving rise to a topological network [Fig. 1(c)]. Like the edge modes at the boundary between two distinct valley topological phases [47–52], the TNMs are protected by the valley topology and robust against the VP defects. Furthermore, this network can be tailored into arbitrary pattern by controlling positions of VM defects, which block transmission in selected channels [Fig. 1(d)], thus provide a unique way to engineer the sound waves. All these extraordinary topological network transports will be demonstrated by our simulation results and experimental data.

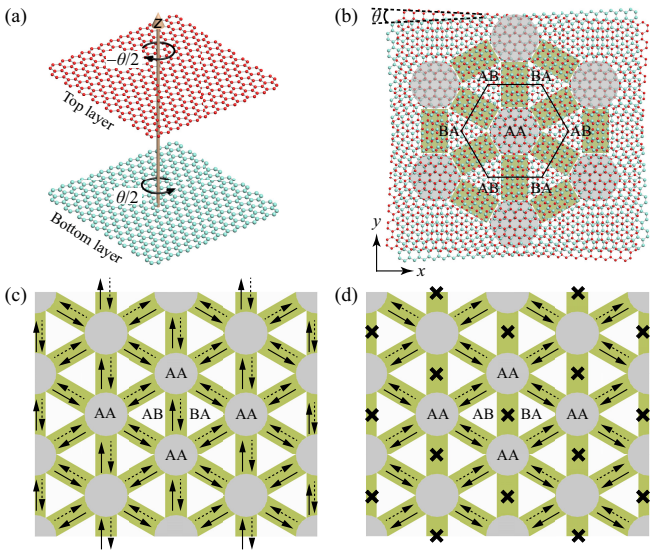

FIG. 1. Approach toward TNMs in TMPCs. (a) Sketch of two acoustic graphene monolayers with Dirac points of different frequencies. (b) Sketch of top view of TMPC with twist angle θ. The black hexagon labels the moiré unit cell, where AB and BA regions are separated by DWs (green). (c) Schematic of topological network for the TNMs confined at DW channels. Arrows in solid (dotted) lines represent the TNMs from the K_0 (K_0') valley. (d) The same as (c), but for the case in the presence of VM defects in y-directional channels, where the defect suppresses the transmission through the corresponding link.

Acoustic TNMs and their topological transports.—Our TMPC is implemented by twisting two coupled 2D acoustic graphene layers for airborne sound. As shown in Fig. 2(a), each acoustic graphene consists of cylindrical cavities (red and cyan) coupled through straight tubes (orange and gray). To obtain the potentials described in the Hamiltonians $H_{\pm}$, the radii of the cavities of the top and bottom acoustic graphene layers are set to $r_1 = 8.2$ and $r = 10$ mm, respectively. Other geometric parameters are chosen as $s = 22$, $d = 8.8$, $d_1 = 4$, $h = 6$ mm and the lattice constant of two acoustic graphene layers are $a = \sqrt{3}s$. With these parameters, each acoustic graphene layer possesses Dirac dispersions, where the Dirac points of the two layers are located at different frequencies [46]. To construct a TMPC with twist angle θ, we first stack these two acoustic graphene layers in z direction and then counterclockwise twist the bottom layer with $\theta/2$ while clockwise twist the top layer with $\theta/2$, as shown in Fig. 1(a). Figure 2(b) presents the unit cell of TMPC with $\theta = 5.085°$, where the configurations of basic AA, AB, and BA stacking types are shown in Fig. 2(c). The interlayer coupling is introduced by uniform white vertical tubes [Figs. 2(b) and 2(c)] of radius $r_0 = 6$ and height $h_1 = 4$ mm for each cavity [46], and its strength depends mostly on the contact area of the top and bottom tubes. The lattice constant of the TMPC is $L = 429.4$ mm and more details can be found in Ref. [46]. Tuned with the interlayer coupling, the regions of AB and BA stacking types develop the same spectral gap (3.69–4.04 kHz) and possess opposite valley Chern numbers [46], which is obtained from the method in Ref. [53]. As proposed in Refs. [16–27,47–50], the topological modes should exist in the DWs between the AB and BA regions. Note that these topological modes are forming a network in our TMPC. To confirm this, we have calculated the band structure of TMPC along several typical directions of moiré Brillouin zone [Fig. 2(c)], as shown in Fig. 2(d). It is distinctly seen that numerous modes (marked in red and blue dots) appear in the band gap

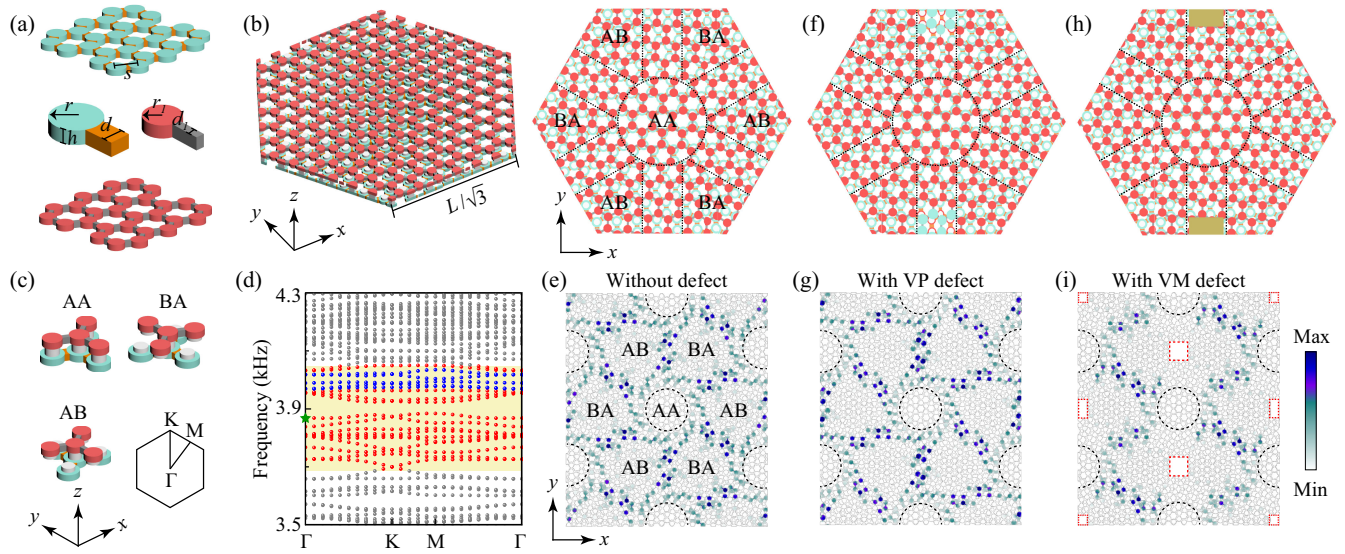

FIG. 2. Numerical demonstrations of the acoustic TNMs and their topological properties. (a) Two acoustic graphene layers for stacking our TMPC. (b) Full and top views of the unit cell of TMPC with $\theta = 5.085°$. (c) Schematic of AA, AB, and BA stackings and the first moiré Brillouin zone. (d) Simulated band structure of the TMPC with $\theta = 5.085°$. The yellow shadow region indicates the band gap of the BA (AB) region (3.69–4.04 kHz). The red (gray) dots indicate the TNMs (bulk modes) and the blue dots indicate the resonant modes. (e) Pressure field distribution for the TNM ($f = 3.87$ kHz) marked by the green star in (d). (f) Top view of the unit cell of TMPC with VP defects located at channels along y direction. (g) The same as (e), but for the TNM of TMPC formed by the unit cell in (f). (h)The same as (f), but for the unit cell with VM defect. (i) The same as (g), but for the TNM of TMPC formed by the unit cell in (h). The red dashed boxes indicate the VM defects. The black dashed circles in (e)–(i) denote the AA regions.

3.69–4.04 kHz (yellow shadow) of the AB and BA regions. As sketched in Fig. 2(e), the modes marked by red dots are confined at DW channels of TMPC, forming a network of triangular lattices. Similar to the topological boundary modes in the bilayer valley topological crystals, the present TNMs span the whole bilayer. Note that the modes marked by blue dots are resonant modes localized away from the AB, BA, and DW regions [46] and not of interest here.

Similar to the topological modes at the boundary between two valley insulators with opposite valley Chern numbers, the TNMs are protected by the valley topology and robust against VP defects [51,54–56]. To elucidate this property, we put the VP defect in the y directional channel in each unit cell [Fig. 2(f)]. The VP defect is constructed by exchanging some cavities of the top layer with those of the bottom layer, see details in Ref. [46]. As demonstrated by the pressure field in Fig. 2(g), TNMs can propagate smoothly along the y directional channels as in the defect free case, forming a perfect network, which gives the possibility to design topological acoustic channels with scatter immunity. Based on the fact that the topological protection of the channels is weak, for strong defects (VM defects) located in the channels, the intervalley scattering could become sizable [16,54,55,57,58], indicating the existence of valley mixing. We then turn to demonstrate that the transmission of the TNMs channel can be blocked by inducing local VM defects. To confirm this, we replace the VP defects with the air cavities [Fig. 2(h)] of size $3s \times 3s \times 2(h + h_1)$ that introduce the valley mixing, see details in Ref. [46]. We find that any link with an air cavity becomes efficiently blocked [Fig. 2(i)] within certain frequency window (3.70–3.89 kHz), which allows us to configure the network into any desired two-dimensional pattern [46], providing a new scheme for controlling acoustic waves. These exceptional performances of topological network transports are of great importance in the fields of information processing and multichannel information transfer.

Experimental observations.—The presence of the TNMs has been directly visualized in our airborne sound experiments. Figure 3(a) shows the experimental sample of size $1472 \times 987 \times 20$ mm fabricated precisely with three-dimensional printing. We have first performed the intensity spectral measurements as a function of frequency to confirm the existence of the band gaps of the AB and BA regions and the TNMs [46]. The experimental intensity spectra detected for three independent experiments are shown in Fig. 3(b). As expected, sizable band gaps are opened in the AB (black) and BA (gray) regions, where band gaps of both regions are the same. The DW spectrum (red) exhibits peak within the band gap, which corresponds exactly to the TNMs. All the spectra are in excellent agreement with predictions of the band dispersion [Fig. 2(d)]. To conclusively confirm the presence of TNMs at the DWs, we perform 2D field profile mapping measurements [46]. Figure 3(c) presents the pressure field of 3.87 kHz measured in the top layer of TMPC. It shows that the sound signal is indeed confined at the DWs and forms a network.

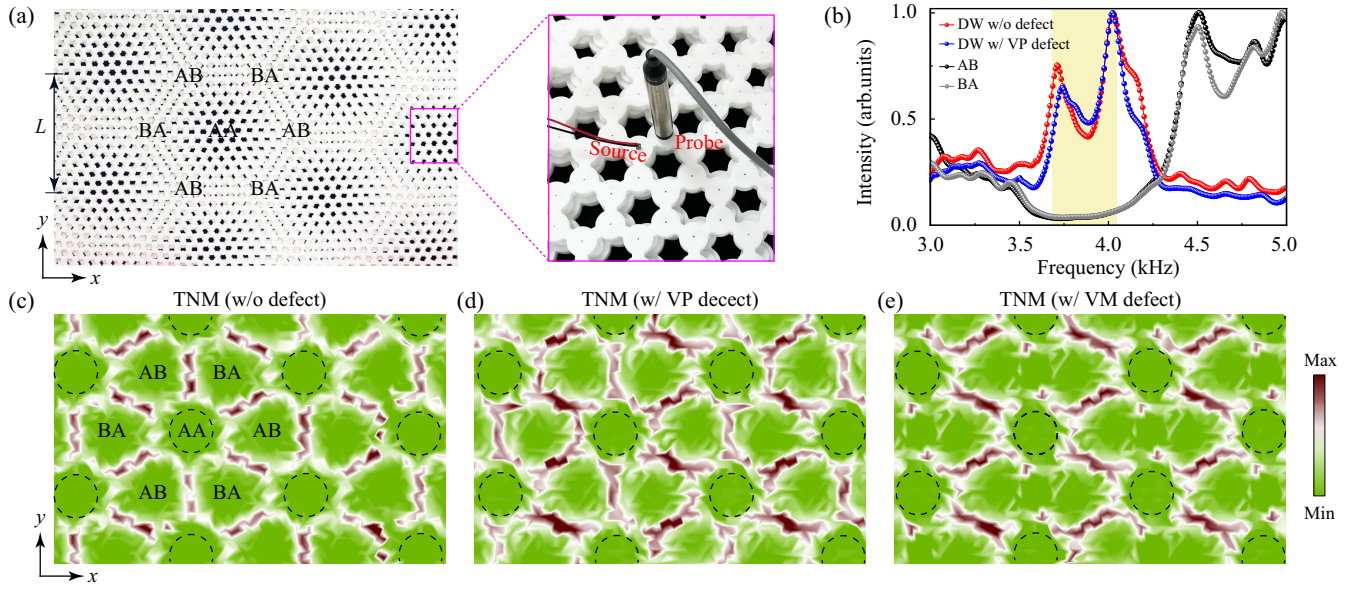

FIG. 3. Experimental identifications of the acoustic TNMs. (a) Photograph of TMPC with $\theta = 5.085°$. The inset amplifies the details of the top layer of sample, on which subwavelength holes are perforated for inserting the sound probe or sound point source. (b) Measured intensity spectra. The black, gray, and red dots indicate the data measured in the AB region, BA region, and y-directional DW of the sample without defects [46], respectively. Blue dots represent the data measured in a y-directional DW of the sample with VP defects [46]. The dips around 3.9 kHz in the DW spectra result from the band gap of TNMs [Fig. 2(d)]. The yellow shadow region indicates the band gap of AB (BA) region (3.69–4.04 kHz). (c) Measured pressure amplitude distribution of TNM at 3.87 kHz. (d) and (e) Same as (c), but for the TMPCs with VP and VM defects in the y-directional channel in each unit cell, respectively. The black dashed circles in (c)–(e) denote the AA regions.

We now turn to confirm the topological robustness of the TNMs against VP defects. The experimental sample with VP defects has the same size as the sample in Fig. 3(a), where the VP defect is introduced in the y directional channel of each moiré unit cell (Fig. S5 of Ref. [46]). In this sample, the transmission through the y directional channel with VP defects will not be blocked and the TNMs transport smoothly through the defect. To confirm this, we have experimentally scanned the pressure field on the top layer of the sample. Figure 3(d) exemplifies the experimental data at 3.87 kHz, where the acoustic wave bypasses the defect and propagates along the prescribed channels, forming a network pattern like the system without the defect. To quantitatively characterize the topological robustness of the TNMs against the VP defects, we further extracted the sound energy at a y directional DW. As shown in Fig. 3(b), the sound intensity spectrum (blue dots) of the VP defect system exhibits almost the same as that of the perfect system (red circles) inside the nontrivial gap region (yellow shadow).

To experimentally demonstrate that the connectivity of the network can be arbitrarily modified by controlling the locations of VM defects, we consider a sample with VM defects which has the same size as that employed in Fig. 3(a). As shown in Fig. S6 in Ref. [46], an air cavity is introduced in the y directional channel of each moiré unit cell. In Fig. 3(e) we present the sound field scanned over the top layer. It shows that sound signals in the y directional channels with VM defects are indeed blocked and propagate only along the perfect channels, forming a new network pattern. We have checked the experimental data and found that any link with an air cavity becomes efficiently blocked [Fig. 3(e)] within a certain frequency window (3.70–3.89 kHz), which agrees well with the simulation results. The field distributions confirm the physical picture introduced in Fig. 1(d): the networks of TNMs can be reconfigured into any desired two-dimensional patterns.

Note that the acoustic TNMs presented here exist in the DWs of TMPC under no external bias fields and structure reconstruction, which are different from the TNMs considered in electronic systems, where the external interlayer bias and structure reconstruction are required. In electronic systems, the large angle twisted moiré electronic system is viewed as decoupled layers, strong interlayer couplings and lattice reconstruction appear only in small angle twisted systems, all of which lead to TNMs appearing only in small angle twisted bilayer graphene systems (e.g., $\theta < 1°$). However, the interlayer couplings of our TMPC can be arbitrarily designed and the structure reconstruction can be precisely controlled. We have constructed a reconstructed TMPC to serve as the analogy of the twisted electronic moiré materials after the lattice reconstruction, which is not discussed in the previously reported artificial moiré systems. Acoustic TNMs are also observed in the DWs of reconstructed structures of TMPCs, see details in Ref. [46].

In this context, the TNMs constructed by our principle can be observed in the DWs of both the unreconstructed and reconstructed TMPC, and can be realized in a wide range of twist angles, as demonstrated by the data in Ref. [46]. Compared to the TNMs recently revealed in monolayer or biaxially strained phononic crystals [37,59] where the TNMs appear in the discrete designed superlattices, the TNMs observed here exhibit more flexibilities in wave manipulations since their network patterns can be smoothly and continuously tuned by twisting operations. We believe that the method proposed here for constructing TNMs is applicable to other classical wave systems, such as electromagnetic and elastic wave systems.

Conclusion.—In summary, we have theoretically proposed and experimentally verified the TNMs in TMPC. Acoustic TNMs propagate along the DWs between AB and BA regions, which are protected by the valley topology. We have demonstrated that the TNMs can be guided without scattering even in the networks with VP defects. Markedly, the VM defects can shut down the transmission through a link due to the valley scattering within a certain frequency, which allows one to modify the connectivity of the network arbitrarily, indicating that TNMs can be guided freely along an arbitrary network path. The capability of freely and topologically routing waves in mass channels is far beyond that exhibited in the early reported conventional waveguides [60–63] or the newly developed topological waveguides [51,52,54–56,58,64–74]. Specifically, for example, compared with topological edge or hinge states which exist only on the one-dimensional boundaries or interfaces and propagate usually along a few straight or specifically shaped channels, the TNMs form a 2D network and can propagate along the network with various shapes. In theoretical aspect, our results will stimulate the investigation of exploring controllable topological phases and valley-dependent phenomena in various classical moiré systems. In application aspect, unique topological network transport offers new possibilities for information communication and energy transportation and presents the possibility to implement the topological device, such as topological beam splitter [46].

This work is supported by the National Key R&D Program of China (No. 2022YFA1404900, No. 2022YFA1404500, No. 2018YFA0305800), National Natural Science Foundation of China (No. 11890701, No. 11974120, No. 11974005, No. 11974262, No. 12074128, No. 12004286, No. 12104347, No. 12222405, No. 12374419, and No. 12374409), Natural Science Foundation of Hubei Province of China (No. 2024AFB712, No. 2023AFB604) and Guangdong Basic and Applied Basic Research Foundation (No. 2021B1515020086, No. 2022B1515020102).

Z. L. and L. Y. initiated the project. D. Y. and L. Y. did the simulations and designed the samples. D. Y., Z. F., Q. W., H. H., L. Y., and M. K. performed the experiments. L. Y., J. L., W. D., X. H., and Z. L. analyzed the data and wrote the manuscript. Z. L. supervised the project. All authors contributed to scientific discussions of the manuscript.

*Corresponding author: lpye@whu.edu.cn
†Corresponding author: zyliu@whu.edu.cn

[1] G. Li, A. Luican, J. M. B. Lopes dos Santos, A. H. Castro Neto, A. Reina, J. Kong, and E. Y. Andrei, Observation of Van Hove singularities in twisted graphene layers, Nat. Phys. **6**, 109 (2009).
[2] R. Bistritzer and A. H. MacDonald, Moiré bands in twisted double-layer graphene, Proc. Natl. Acad. Sci. U.S.A. **108**, 12233 (2011).
[3] I. Brihuega, P. Mallet, H. Gonzalez-Herrero, G. Trambly de Laissardiere, M. M. Ugeda, L. Magaud, J. M. Gomez-Rodriguez, F. Yndurain, and J. Y. Veuillen, Unraveling the intrinsic and robust nature of van Hove singularities in twisted bilayer graphene by scanning tunneling microscopy and theoretical analysis, Phys. Rev. Lett. **109**, 196802 (2012).
[4] C. Zhang, C.-P. Chuu, X. Ren, M.-Y. Li, L.-J. Li, C. Jin, M.-Y. Chou, and C.-K. Shih, Interlayer couplings, Moiré patterns, and 2D electronic superlattices in MoS2/WSe2 hetero-bilayers, Sci. Adv. **3**, e1601459 (2017).
[5] Y. Cao, V. Fatemi, A. Demir, S. Fang, S. L. Tomarken, J. Y. Luo, J. D. Sanchez-Yamagishi, K. Watanabe, T. Taniguchi, E. Kaxiras *et al.*, Correlated insulator behaviour at half-filling in magic-angle graphene superlattices, Nature (London) **556**, 80 (2018).
[6] Y. Cao, V. Fatemi, S. Fang, K. Watanabe, T. Taniguchi, E. Kaxiras, and P. Jarillo-Herrero, Unconventional superconductivity in magic-angle graphene superlattices, Nature (London) **556**, 43 (2018).
[7] K. L. Seyler, P. Rivera, H. Yu, N. P. Wilson, E. L. Ray, D. G. Mandrus, J. Yan, W. Yao, and X. Xu, Signatures of moiré-trapped valley excitons in $MoSe_2/WSe_2$ heterobilayers, Nature (London) **567**, 66 (2019).
[8] K. Tran, G. Moody, F. Wu, X. Lu, J. Choi, K. Kim, A. Rai, D. A. Sanchez, J. Quan, A. Singh *et al.*, Evidence for moiré excitons in van der Waals heterostructures, Nature (London) **567**, 71 (2019).
[9] S. Chen, M. He, Y.-H. Zhang, V. Hsieh, Z. Fei, K. Watanabe, T. Taniguchi, D. H. Cobden, X. Xu, C. R. Dean, and M. Yankowitz, Electrically tunable correlated and topological states in twisted monolayer–bilayer graphene, Nat. Phys. **17**, 374 (2020).
[10] M. Serlin, C. L. Tschirhart, H. Polshyn, Y. Zhang, J. Zhu, K. Watanabe, T. Taniguchi, L. Balents, and A. F. Young, Intrinsic quantized anomalous Hall effect in a moiré heterostructure, Science **367**, 900 (2020).
[11] S. Carr, S. Fang, and E. Kaxiras, Electronic-structure methods for twisted moiré layers, Nat. Rev. Mater. **5**, 748 (2020).
[12] Y. Wang, J. Herzog-Arbeitman, G. W. Burg, J. Zhu, K. Watanabe, T. Taniguchi, A. H. MacDonald, B. A. Bernevig, and E. Tutuc, Bulk and edge properties of twisted double bilayer graphene, Nat. Phys. **18**, 48 (2021).

[13] A. Ghiotto, E.-M. Shih, G. S. S. G. Pereira, D. A. Rhodes, B. Kim, J. Zang, A. J. Millis, K. Watanabe, T. Taniguchi, J. C. Hone *et al.*, Quantum criticality in twisted transition metal dichalcogenides, Nature (London) **597**, 345 (2021).
[14] C. R. Woods, P. Ares, H. Nevison-Andrews, M. J. Holwill, R. Fabregas, F. Guinea, A. K. Geim, K. S. Novoselov, N. R. Walet, and L. Fumagalli, Charge-polarized interfacial superlattices in marginally twisted hexagonal boron nitride, Nat. Commun. **12**, 347 (2021).
[15] H. Yang, L. Liu, H. Yang, Y. Zhang, X. Wu, Y. Huang, H.-J. Gao, and Y. Wang, Advance in two-dimensional twisted moiré materials: Fabrication, properties, and applications, Nano Res. **16**, 2579 (2022).
[16] P. San-Jose and E. Prada, Helical networks in twisted bilayer graphene under interlayer bias, Phys. Rev. B **88**, 121408(R) (2013).
[17] D. K. Efimkin and A. H. MacDonald, Helical network model for twisted bilayer graphene, Phys. Rev. B **98**, 035404 (2018).
[18] M. Anđelković, L. Covaci, and F. M. Peeters, DC conductivity of twisted bilayer graphene: Angle-dependent transport properties and effects of disorder, Phys. Rev. Mater. **2**, 034004 (2018).
[19] P. Rickhaus, J. Wallbank, S. Slizovskiy, R. Pisoni, H. Overweg, Y. Lee, M. Eich, M.-H. Liu, K. Watanabe, T. Taniguchi *et al.*, Transport through a network of topological channels in twisted bilayer graphene, Nano Lett. **18**, 6725 (2018).
[20] S. Huang, K. Kim, D. K. Efimkin, T. Lovorn, T. Taniguchi, K. Watanabe, A. H. MacDonald, E. Tutuc, and B. J. LeRoy, Topologically protected helical states in minimally twisted bilayer graphene, Phys. Rev. Lett. **121**, 037702 (2018).
[21] A. Ramires and J. L. Lado, Electrically tunable gauge fields in tiny-angle twisted bilayer graphene, Phys. Rev. Lett. **121**, 146801 (2018).
[22] H. Yoo, R. Engelke, S. Carr, S. Fang, K. Zhang, P. Cazeaux, S. H. Sung, R. Hovden, A. W. Tsen, T. Taniguchi *et al.*, Atomic and electronic reconstruction at the van der Waals interface in twisted bilayer graphene, Nat. Mater. **18**, 448 (2019).
[23] S. G. Xu, A. I. Berdyugin, P. Kumaravadivel, F. Guinea, R. K. Kumar, D. A. Bandurin, S. V. Morozov, W. Kuang, B. Tsim, S. Liu *et al.*, Giant oscillations in a triangular network of one-dimensional states in marginally twisted graphene, Nat. Commun. **10**, 4008 (2019).
[24] M. Fleischmann, R. Gupta, F. Wullschlager, S. Theil, D. Weckbecker, V. Meded, S. Sharma, B. Meyer, and S. Shallcross, Perfect and controllable nesting in minimally twisted bilayer graphene, Nano Lett. **20**, 971 (2020).
[25] Y.-W. Liu, Y. Su, X.-F. Zhou, L.-J. Yin, C. Yan, S.-Y. Li, W. Yan, S. Han, Z.-Q. Fu, Y. Zhang *et al.*, Tunable lattice reconstruction, triangular network of chiral one-dimensional states, and bandwidth of flat bands in magic angle twisted bilayer graphene, Phys. Rev. Lett. **125**, 236102 (2020).
[26] J. D. Verbakel, Q. Yao, K. Sotthewes, and H. J. W. Zandvliet, Valley-protected one-dimensional states in small-angle twisted bilayer graphene, Phys. Rev. B **103**, 165134 (2021).
[27] B. Tsim, N. N. T. Nam, and M. Koshino, Perfect one-dimensional chiral states in biased twisted bilayer graphene, Phys. Rev. B **101**, 125409 (2020).
[28] Y. Deng, M. Oudich, N. JRK. Gerard, J. Ji, M. Lu, and Y. Jing, Magic-angle bilayer phononic graphene, Phys. Rev. B **102**, 180304(R) (2020).
[29] M. R. Lopez, F. Penaranda, J. Christensen, and P. San-Jose, Flat bands in magic-angle vibrating plates, Phys. Rev. Lett. **125**, 214301 (2020).
[30] W. Wang, W. Gao, X. Chen, F. Shi, G. Li, J. Dong, Y. Xiang, and S. Zhang, Moiré fringe induced gauge field in photonics, Phys. Rev. Lett. **125**, 203901 (2020).
[31] G. Hu, A. Krasnok, Y. Mazor, C.-W. Qiu, and A. Alu, Moiré hyperbolic metasurfaces, Nano Lett. **20**, 3217 (2020).
[32] B. Lou, N. Zhao, M. Minkov, C. Guo, M. Orenstein, and S. Fan, Theory for twisted bilayer photonic crystal slabs, Phys. Rev. Lett. **126**, 136101 (2021).
[33] M. Oudich, G. Su, Y. Deng, W. Benalcazar, R. Huang, N. JRK. Gerard, M. Lu, P. Zhan, and Y. Jing, Photonic analog of bilayer graphene, Phys. Rev. B **103**, 214311 (2021).
[34] K. Dong, T. Zhang, J. Li, Q. Wang, F. Yang, Y. Rho, D. Wang, C. P. Grigoropoulos, J. Wu, and J. Yao, Flat bands in magic-angle bilayer photonic crystals at small twists, Phys. Rev. Lett. **126**, 223601 (2021).
[35] H. Tang, F. Du, S. Carr, C. DeVault, O. Mello, and E. Mazur, Modeling the optical properties of twisted bilayer photonic crystals, Light Sci. Appl. **10**, 157 (2021).
[36] S M. Gardezi, H. Pirie, S. Carr, W. Dorrell, and J. E Hoffman, Simulating twistronics in acoustic metamaterials, 2D Mater. **8**, 031002 (2021).
[37] S. Zheng, J. Zhang, G. Duan, Z. Jiang, X. Man, D. Yu, and B. Xia, Topological network and valley beam splitter in acoustic biaxially strained moiré superlattices, Phys. Rev. B **105**, 184104 (2022).
[38] C.-H. Yi, H. C. Park, and M. J. Park, Strong interlayer coupling and stable topological flat bands in twisted bilayer photonic moiré superlattices, Light **11**, 289 (2022).
[39] S.-Q. Wu, Z.-K. Lin, B. Jiang, X. Zhou, Z. Hang, B. Hou, and J.-H. Jiang, Higher-order topological states in acoustic twisted moiré superlattices, Phys. Rev. Appl. **17**, 034061 (2022).
[40] G. Duan, S. Zheng, J. Zhang, Z. Jiang, X. Man, D. Yu, and B. Xia, Synthetic gauge fields and Landau levels in acoustic moiré superlattices, Appl. Phys. Lett. **123**, 021702 (2023).
[41] L. Huang, W. Zhang, and X. Zhang, Moiré quasibound states in the continuum, Phys. Rev. Lett. **128**, 253901 (2022).
[42] I. Nasidi, R. Hao, S. Jin, and E. Li, Flat bands and quasi-bound states in the continuum in a photonic Moiré lattice, J. Opt. Soc. Am. B **40**, 260 (2023).
[43] P. Wang, Y. Zheng, X. Chen, C. Huang, Y. V. Kartashov, L. Torner, V. V. Konotop, and F. Ye, Localization and delocalization of light in photonic moire lattices, Nature (London) **577**, 42 (2020).
[44] Q. Fu, P. Wang, C. Huang, Y. V. Kartashov, L. Torner, V. V. Konotop, and F. Ye, Optical soliton formation controlled by angle twisting in photonic moiré lattices, Nat. Photonics **14**, 663 (2020).
[45] Z. Jiang, J. Liu, S. Zheng, G. Duan, and B. Xia, Phononic twisted moiré lattice with quasicrystalline patterns, Appl. Phys. Lett. **121**, 142202 (2022).
[46] See Supplemental Material at http://link.aps.org/supplemental/10.1103/PhysRevLett.132.266602 for more details on the Berry curvature, TNMs in reconstructed

TMPC, TNMs in 3.89° and methods of simulations and experiments.

[47] F. Zhang, A. H. MacDonald, and E. J. Mele, Valley Chern numbers and boundary modes in gapped bilayer graphene, Proc. Natl. Acad. Sci. U.S.A. **110**, 10546 (2013).

[48] A. Vaezi, Y. Liang, D. H. Ngai, L. Yang, and E.-A. Kim, Topological edge states at a tilt boundary in gated multilayer graphene, Phys. Rev. X **3**, 021018 (2013).

[49] L. Ju, Z. Shi, N. Nair, Y. Lv, C. Jin, J. V. Jr., C. Ojeda-Aristizabal, H. A. Bechtel, M. C. Martin, A. Zettl *et al.*, Topological valley transport at bilayer graphene domain walls, Nature (London) **520**, 650 (2015).

[50] L.-J. Yin, H. Jiang, J.-B. Qiao, and L. He, Direct imaging of topological edge states at a bilayer graphene domain wall, Nat. Commun. **7**, 11760 (2016).

[51] J. Lu, C. Qiu, L. Ye, X. Fan, M. Ke, F. Zhang, and Z. Liu, Observation of topological valley transport of sound in sonic crystals, Nat. Phys. **13**, 369 (2016).

[52] J. Lu, C. Qiu, W. Deng, X. Huang, F. Li, F. Zhang, S. Chen, and Z. Liu, Valley topological phases in bilayer sonic crystals, Phys. Rev. Lett. **120**, 116802 (2018).

[53] T. Fukui, Y. Hatsugai, and H. Suzuki, Chern numbers in discretized brillouin zone: Efficient method of computing (spin) Hall conductances, J. Phys. Soc. Jpn. **74**, 1674 (2005).

[54] M. Yan, J. Lu, F. Li, W. Deng, X. Huang, J. Ma, and Z. Liu, On-chip valley topological materials for elastic wave manipulation, Nat. Mater. **17**, 993 (2018).

[55] Z. Zhang, Y. Tian, Y. Cheng, Q. Wei, X. Liu, and J. Christensen, Topological acoustic delay line, Phys. Rev. Appl. **9**, 034032 (2018).

[56] M. Wang, W. Zhou, L. Bi, C. Qiu, M. Ke, and Z. Liu, Valley-locked waveguide transport in acoustic heterostructures, Nat. Commun. **11**, 3000 (2020).

[57] B. R. Matis, B. H. Houston, and J. W. Baldwin, Low-energy resonant scattering from hydrogen impurities in graphene, Phys. Rev. B **88**, 085441 (2013).

[58] P. Gao, Z. Zhang, and J. Christensen, Sonic valley-Chern insulators, Phys. Rev. B **101**, 020301(R) (2020).

[59] R. Zheng, M. Yan, J. Wu, W. Deng, J. Lu, X. Huang, and Z. Liu, Topological network transport in on-chip phononic crystals, Phys. Rev. B **107**, 245122 (2023).

[60] S.-Y. Lin, E. Chow, V. Hietala, P. R. Villeneuve, and J. D. Joannopoulos, Experimental demonstration of guiding and bending of electromagnetic waves in a photonic crystal, Science **282**, 274 (1998).

[61] A. Khelif, A. Choujaa, S. Benchabane, B. Djafari-Rouhani, and V. Laude, Guiding and bending of acoustic waves in highly confined phononic crystal waveguides, Appl. Phys. Lett. **84**, 4400 (2004).

[62] Y. A. Vlasov, M. O Boyle, H. F. Hamann, and S. J. McNab, Active control of slow light on a chip with photonic crystal waveguides, Nature (London) **438**, 65 (2005).

[63] A. Khelif and A. Adibi, *Phononic Crystals: Fundamentals and Applications* (Springer, New York 2016).

[64] Z. Wang, Y. Chong, J. D. Joannopoulos, and M. Soljacic, Observation of unidirectional backscattering-immune topological electromagnetic states, Nature (London) **461**, 772 (2009).

[65] M. C. Rechtsman, J. M. Zeuner, Y. Plotnik, Y. Lumer, D. Podolsky, F. Dreisow, S. Nolte, M. Segev, and A. Szameit, Photonic Floquet topological insulators, Nature (London) **496**, 196 (2013).

[66] R. Susstrunk and S. D. Huber, Observation of phononic helical edge states in a mechanical topological insulator edge states in a mechanical topological insulator, Science **349**, 47 (2015).

[67] C. He, X. Ni, H. Ge, X.-C. Sun, Y.-B. Chen, M.-H. Lu, X.-P. Liu, and Y.-F. Chen, Acoustic topological insulator and robust one-way sound transport, Nat. Phys. **12**, 1124 (2016).

[68] F. Li, X. Huang, J. Lu, J. Ma, and Z. Liu, Weyl points and Fermi arcs in a chiral phononic crystal, Nat. Phys. **14**, 30 (2017).

[69] J. Cha, K. W. Kim, and C. Daraio, Experimental realization of on-chip topological nanoelectromechanical metamaterials, Nature (London) **564**, 229 (2018).

[70] C. He, S.-Y. Yu, H. Ge, H. Wang, Y. Tian, H. Zhang, X.-C. Sun, Y. B. Chen, J. Zhou, M.-H. Lu *et al.*, Three-dimensional topological acoustic crystals with pseudospin-valley coupled saddle surface states, Nat. Commun. **9**, 4555 (2018).

[71] H. He, C. Qiu, L. Ye, X. Cai, X. Fan, M. Ke, F. Zhang, and Z. Liu, Topological negative refraction of surface acoustic waves in a Weyl phononic crystal, Nature (London) **560**, 61 (2018).

[72] X. Zhang, B.-Y. Xie, H.-F. Wang, X. Xu, Y. Tian, J.-H. Jiang, M.-H. Lu, and Y.-F. Chen, Dimensional hierarchy of higher-order topology in three-dimensional sonic crystals, Nat. Commun. **10**, 5331 (2019).

[73] L. Luo, H.-X. Wang, Z.-K. Lin, B. Jiang, Y. Wu, F. Li, and J.-H. Jiang, Observation of a phononic higher-order Weyl semimetal, Nat. Mater. **20**, 794 (2021).

[74] Q. Wei, X. Zhang, W. Deng, J. Lu, X. Huang, M. Yan, G. Chen, Z. Liu, and S. Jia, Higher-order topological semimetal in acoustic crystals, Nat. Mater. **20**, 812 (2021).